X-FEM for Abaqus (XFA) Toolkit for Automated Crack Onset and Growth Simulation: New Development, Validation, and Demonstration

Jay Shi[1], Jim Lua[2], Liguo Chen[3], David Chopp[4], and N. Sukumar[5]

Global Engineering and Materials, Inc.
[1]jshi@gem-consultant.com
[2]jlua@gem-consultant.com
[3]lgchen@gem-consultant.com

[4]Northwestern University
chopp@northwestern.edu

[5]University of California at Davis
nsukumar@ucdavis.edu

Abstract: *A software tool for automated crack onset and growth simulation based on the eXtended Finite Element Method (X-FEM) is developed. This XFA tool for the first time is able to simulate arbitrary crack growth or composite delamination without remeshing. The automated tool is integrated with Abaqus/Standard and Abaqus/CAE via the customization interfaces. It seamlessly works with the Commercial, Off-The-Shelf (COTS) Abaqus suite. Its unique features include: 1) CAE-based insertion of 3D multiple cracks with arbitrary shape of crack front that is independent of an existing mesh; 2) simulation of crack growth inside or between solid elements; 3) simulation of non self-similar crack growth along an arbitrary path or a user-specified interface; 4) extraction of G/K parameters via the modified VCCT, cohesive method, or CTOD; and 5) CAE-based data processing and visualization. The G/K predictions agree very well with published results using the conventional, double-node model and domain integration method. The toolkit can be used for the following simulation needs: 1) crack propagation, fatigue life prediction, multiple crack interaction, and sensitivity analysis and design optimization; 2) 2D or 3D solid model in quasi-static, monotonic or fatigue loading; 3) metallic fracture or composite delamination;4) elastic The usability of the toolkit is illustrated through a series of industrial problems.*

Keywords: *X-FEM, VCCT, Fatigue, Fracture & Failure, Crack Growth, Delamination, Abaqus/Standard, UEL*

1. Introduction

Damage tolerance design requires a structure to withstand sub-critical growth of manufacturing flaws and service-induced defects against failure. Traditionally the analysis is done by handbook lookup or using simplified models with empirical parameters. This approach is not adequate for unitized structures featuring complex geometric details and loading conditions. Given the escalating costs associated with the test-driven certification and qualification procedures, there is an immediate need for verified computational software to perform crack growth simulation under monotonic and cyclic loading. Global Engineering and Materials, Inc. (GEM) along with our team members (SIMULIA, LM Aero and Caterpillar) and our consultants (Professor Ted Belytschko, Professor N. Sukumar, and Professor David Chop) have developed an eXtended Finite Element Method (XFEM) coupled with Fast Marching Method (FMM) for simulation of 3D curvilinear crack growth with an arbitrary front shape [1][2]. The resulting tool can be used to assess the residual strength and fatigue life of a structure with multiple cracks. This automated crack growth prediction tool is implemented within the Abaqus implicit solver. It will not only capture the commonly accepted and understood failure physics but be consistent with current damage tolerance and residual strength assessment requirements and testing procedures. The tool features 1) arbitrary insertion of multiple initial cracks that are independent of an existing finite element mesh; 2) characterization of a moving crack without remeshing; 3) accurate prediction of crack evolution using mixed-mode crack growth criteria under fatigue and monotonic loading; and 4) characterization of crack closure via a frictional contact algorithm.

This paper is intended to present our recent developments in XFEM and demonstrate its capability using a series of real examples from industries.

2. Automatic Element Slicing

The element slicing, or element partition, is the key component to perform numerical integration in X-FEM element when the element is cut by a crack surface. In particular, a 3-dimensional finite element is to be sliced by an arbitrary plane that is given by a point on it and its bi-normal (to the crack plane). Because of discontinuities in enrichment functions, when volume integration is performed, the finite element must be subdivided into regions in which displacement field is continuous and Gauss quadrature can be utilized within each region for the integration. The sub-elements and sub-nodes that are generated during slicing can also be used in the post-processing to visualize the crack opening and the deformed shape of the FEM model just as in the regular finite elements. The 3D element slicing is critical in the element-based weak form evaluation and has not been fully studied in the literature. In a recent paper by Sukumar of UC Davis, the element sliced by a planar surface is considered. However, the slicing for tip element (partially sliced with crack front embedded in the element) is not considered. Furthermore, the bilinear crack surface (recovered by nodal level set values and the linear shape functions of the underline element) slicing has not found in literature. The accurate cut representation of the X-FEM element by a nonplanar crack surface is pivotal to the 3D crack simulation for arbitrary growth pattern.

We have extended the element slicing algorithm for both complete cut and partial cut cases. The volume integration of the X-FEM element is considered as contribution from each tetra elements (sub-elements), which are in turn calculated by Gauss quadrature. In the following table the volume and an analytical test function are estimated using the element slicing and the resulting Gauss points. The exact solutions were achieved using our 3D slicing algorithm. The element slicing was integrated in the 3D element code for two different purposes: assigning integration points confirming to crack configuration, and providing subsidiary mesh to visualize deformation and other results inside the XFEM region.

After the element slicing, the final mesh for visualization purpose can be seen in the following figure. Very different from adaptive remeshing, in XFEM's slicing scheme, each element being cut by a crack surface is subdivided into a series of tetra elements, or sub elements to allow consistent integration point assignment; therefore the slicing is performed in the individual XFEM element and it can be implemented as part of the iso-parametric element subroutine (a.k.a. much faster and easier to implemented). Secondly, the Gauss points are associated with the original brick element, not the tetrahedral sub elements. The brick element shape functions are used and the volume integration is also performed for the whole brick element. So the numerical integration scheme is still based on the underline brick element, not a series of tetra elements. This is the fundamental difference between the slicing scheme and the adaptive remeshing scheme.

The following figure shows the positioning of the crack surface that cuts a simple, brick solid model. The example features a curved (half elliptical) crack front shown in the figure below:

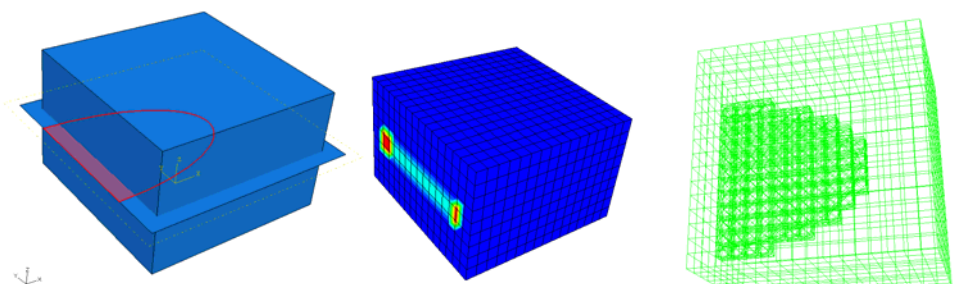

Figure 1: Interaction of Solid Model and Crack Surface Mesh.

In this example the reference surface cuts the brick geometry in the middle. Next, the highlighted region of the reference surface is specified by the user as the actual crack surface. Because the crack surface extends beyond the brick boundary, this would define an edge crack.

The solid mesh of the brick geometry and the shell (using triangular shell: S3) mesh are the two inputs required to generate the initial level set value and XFEM pre-processing. The following figure shows the number of activated nodal DOFs. For the tip elements (containing the crack front), all nodes will be tip-enriched with the four branch functions, thus totaling 15 DOFs, as the red region in the figure. For the cut elements (containing part of the crack surface that cuts completely the element volume), the jump enrichment function is activated, therefore having a total of 6 DOFs per node (the light green region). Finally for elements that does not share a cut by the crack. The regular integration scheme is used and only 3 DOFs are activated per node (the blue region).

Slice the crack surface in the way similar to the 2D quad element; then resume the 3D slicing based on the sub-nodes generated by the 2D slicing:

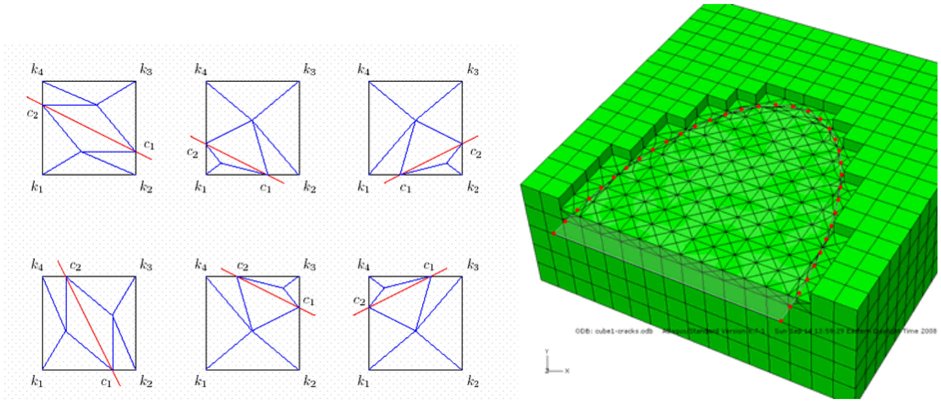

Figure 2: Slicing Scheme of Solid Element Mesh.

3. Extend Fast Marching Method for Multiple Crack simulation

The fast marching method coupled with the extended finite element method is commonly used for crack modeling [5]. The initial crack geometry is represented by two level set functions (one for the crack surface, second to locate the crack tip) and subsequently signed distance functions are used to maintain the location of the crack. Some people refer to this as vector level set methods [6]. The level sets are updated by solving hyperbolic PDEs using fast marching method.

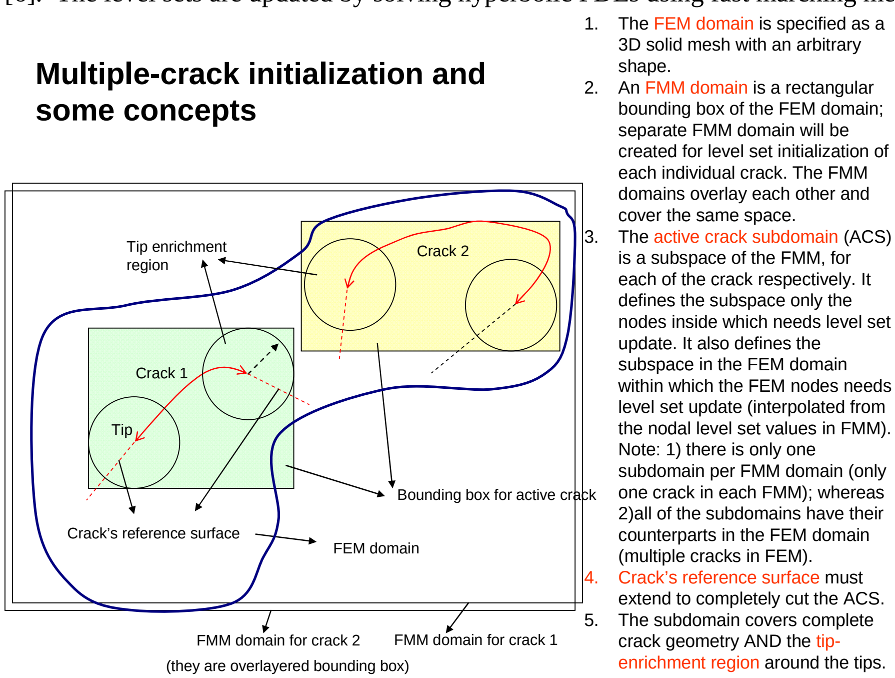

Figure 3: Multiple-Crack Level Set Initialization and Some Concepts

One limitation of this technique is that it can only model one crack in single domain, but in real situations, two or more cracks often coexist, and they may or may not have interactions with each other. So our goal is to extend this FMM and XFEM coupled technique to model multiple cracks in single domain. Initially, there is no interaction between the cracks.

Based on the philosophy of vector level sets methods, we simply adding another group of level sets function and model the cracks one by one. For two cracks, we will have two groups of vector level sets for single domain. It will cause problems to calculate enrichment function in XFEM since there will be two sets of data. In order to solve this dilemma, we divide the single domain into multiple zones, usually each crack will own a zone and then the rest belong to a zone. Then in the zones with a crack, a group of vector level set will be used to describe the location of crack and signed distance functions. There is one overlapping between zones, which will make sure that in one location, the level set functions are unique for each vector level set component.

4. XFA Tool Validation

4.1 Validation 1: The accuracy of the fatigue crack growth path and fatigue life prediction [3].

This example features a modified CT specimen, in which a hole is inserted in order to produce stress concentration, so that a fatigue crack path curves toward the hole. The tested material was a cold rolled SAE 1020 steel, with the analyzed weight percent composition: C 0.19, Mn 0.46, Si 0.14, Ni 0.052, Cr 0.045, Mo 0.007, Cu 0.11, Nb 0.002, Ti 0.002, Fe balance. The Young's modulus is E = 205 GPa; the yield strength is 285 MPa, the ultimate strength is 491 MPa, and the area reduction 53.7%. These properties are measured according to the ASTM E 8M-99 standard. The da=dN vs. dK data, also obtained under a stress ratio r=0.1 and measured following ASTM E647-99 procedures, is fitted by the modified Elber equation: $\frac{da}{dN} = 4.5 \cdot 10^{-10} \cdot (\Delta K - \Delta K_{th})^{2.1}$, where dK=11.6MPa is the threshold stress-intensity range. The specimen geometry, hole configuration, fatigue load, and material property are summarized in Figure 4.

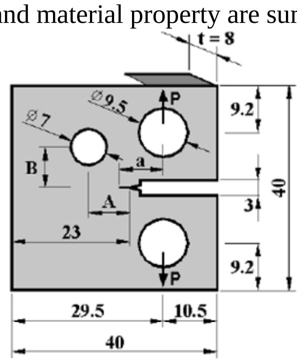

	A	B
CT1(CA)	8.3	8.1
CT2(CA)	8.4	6.9
CT1(VA)	8.3	8.1

Determine P such that

ΔK_I=20MPa $m^{1/2}$, R=0.1

(a)

- SAE 1020 Steel
  - Yield strength = 285 MPa
  - Poisson's Ratio =0.3
  - Ultimate Strength = 491 MPa
  - Young's Modulus = 205 GPa
  - Fracture toughness (Kc) = 280 MPam1/2
  - DK0=11.5 MPa m1/2

w= 29.5 mm
t= 8 mm

Applied Stress = P/wt

Figure 4: CT1 and CT2 Fatigue Specimen Set-ups

The applied load, P, is such that the dK per cycle is maintained at about 20MPa. Since we cannot determine dK a priori, the load curve used by the paper was interpolated and used in the XFEM simulation. The load history is shown in the following figure:

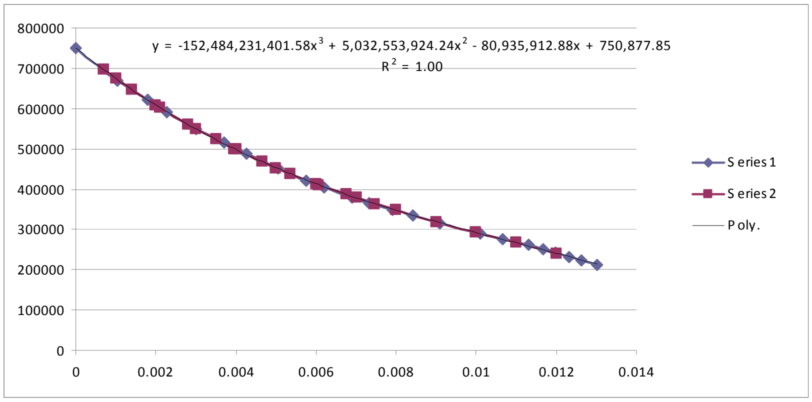

Figure 5: Load P Magnitude Curve as a Function of the Crack Extension Size

For the CT1 specimen, the crack path for coarse mesh and the fine mesh is shown in the Figure 6. A small mesh sensitivity is observed (right-top plot shows the crack tip trajectory). Virtually no dependence of the crack growth step size, da, was found on this particular example (right-bottom plot shows the crack tip trajectory corresponding to da=1.0mm and da=0.7mm).

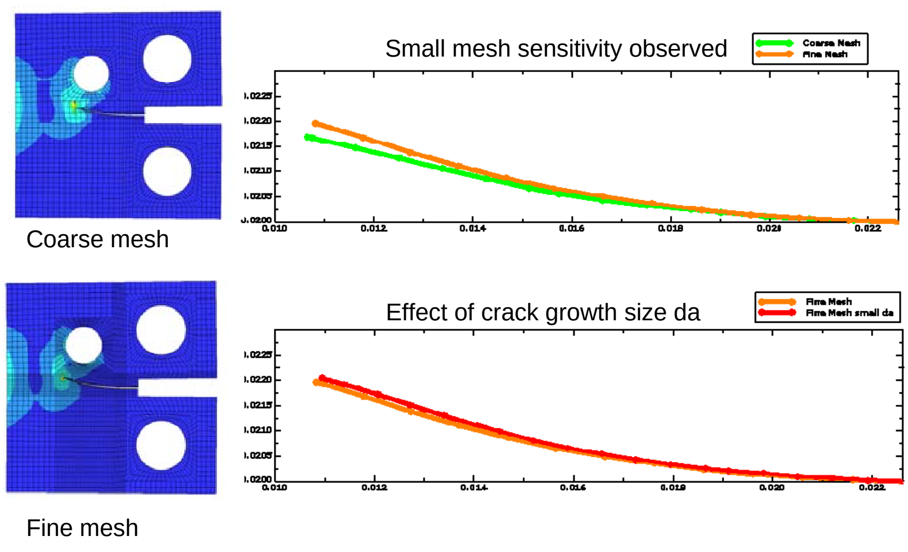

Figure 6: Mesh Sensitivity Study and Path Dependence on Crack Growth Size da.

The predictions indicated that the fatigue crack was always attracted by the hole, but it could either curve its path and grow toward the hole or just be deflected by the hole and continue to propagate after missing it. The XFEM-predicted KI, the KI values predicted by the adaptive remeshing in the reference paper are presented and compared to the standard CTS values in the following Figure 7:

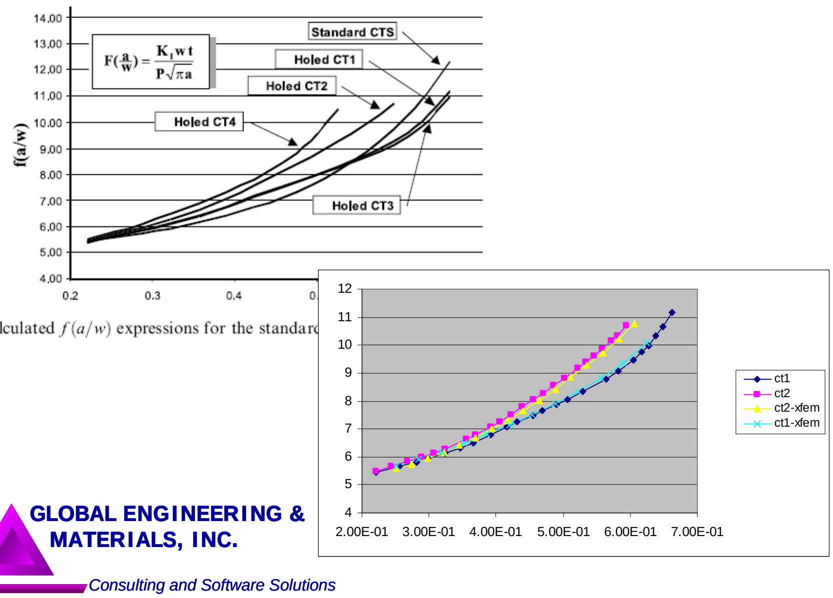

Figure 7: Fatigue Life Geometric Factor as Function of Crack Extension Size

For both CT1 and CT2 specimen the KI prediction matches with the reference results very well.

Next, the da-dN curves for XFEM prediction was also plotted against the reference paper results and the experiments as in Figure 8. It is noted the da-dN curve follows exactly the paper's simulation because the same loading history curve has been used.

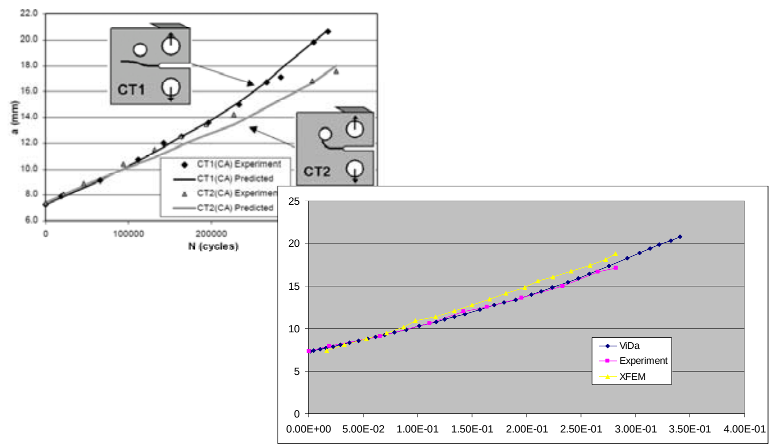

Figure 8: da-dN Curve for CT Specimens

The Von Mises stress contour at various time steps and crack configurations are plotted in Figure 9. The crack starts straight; then turns upward to the hole.

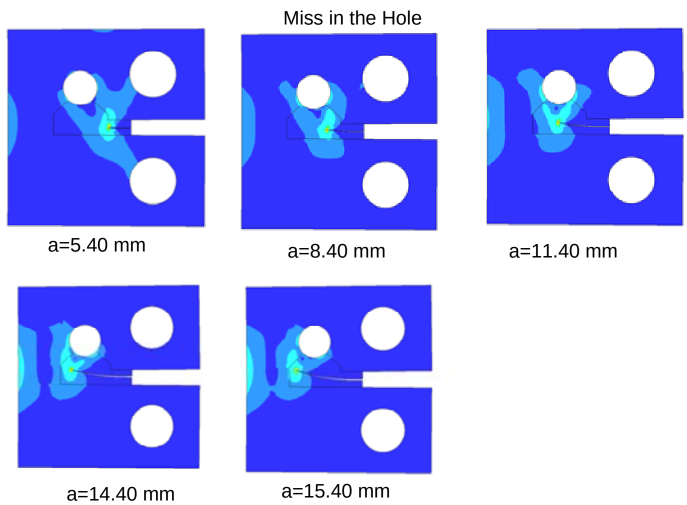

Figure 9: Snapshots of Crack Path and Mises Stress in Deformed Shape.

In CT2 specimen, the center of the attraction hole was lowered from 8.10mm (CT1) to 6.90mm (CT2) to further curve the crack path. Similar to CT1 case, we also use both a coarse mesh and a refined mesh to investigate the path dependence on the mesh (Figure 10).

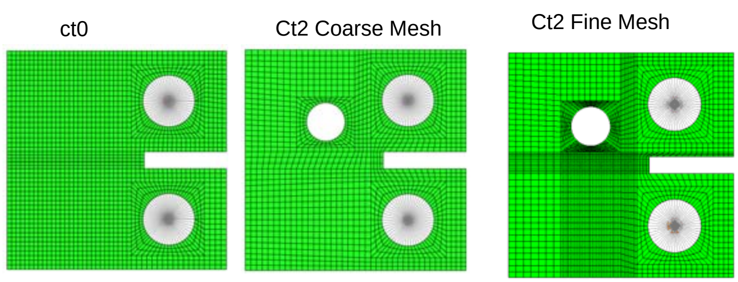

Figure 10: CT2 (Sink-Hole) Specimen FEM Models

The load curve was also interpolated from the paper, assuming for each cycle, the dK maintains at 20MPa range.

For this case small mesh sensitivity to the crack growth path was also observed; however, the crack growth step size, da, seems to have certain effects on the crack trajectory, as shown in Figure 11.

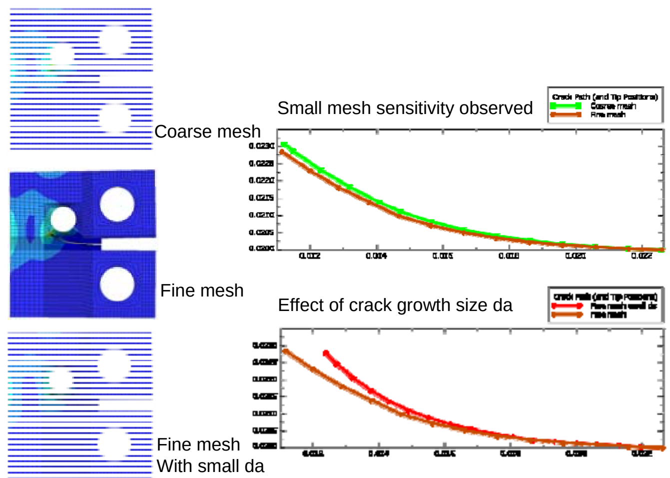

Figure 11: Mesh Sensitivity Study and Path Dependence on Crack Growth Size da.

The crack path predicted by XFEM matches very well with both the simulation and experiments from the reference paper (Figure 12):

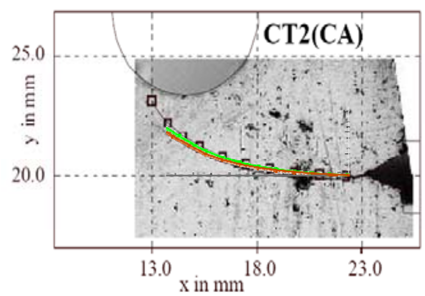

Figure 12: Fatigue Crack Path Prediction by XFEM vs Experiment Image

Finally, the stress contours at different snapshots are plotted in Figure 13. Compared to CT1, the crack is attracted toward the hole with larger curvature.

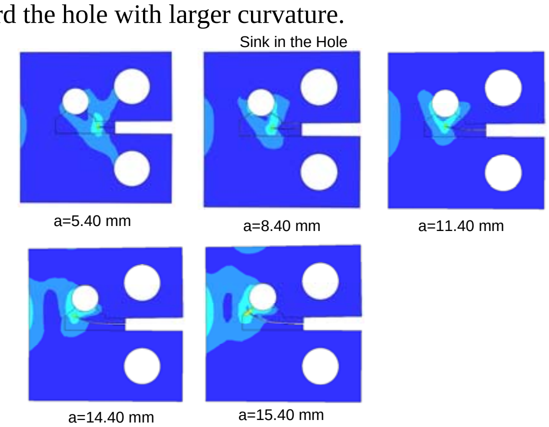

Figure 13: Snapshots of Crack Path and Mises Stress in Deformed Shape.

4.2 Validation 2: Composite joint penny-shape delamination study to demonstrate the importance of considering crack closure in shear-dominant type of delamination crack analysis.

For a typical composite joint model, a large penny-shape crack is embedded in the skin area (Figure 14). The mesh design for both X-FEM and double-node reference model is also shown in the figure. The ray-mesh is required in the double-node model to extract accurate G values. The same mesh is used in X-FEM because of two reasons: 1) it eliminates any discrepancies coming from mesh dependence; 2) currently we only use the jump enrichment so the crack front can only goes along the element boundaries. This is certainly no the limitation of X-FEM.

The nodal enrichment layout is illustrated in the top-right part of the figure. At the tip nodes (blue dots) the jump enrichments are assigned. The jump enrichment DOF is then associated with a large penalty stiffness to close the crack. The conjugate force is the tip force. The pink dots are the behind-tip nodes. The nodes are also jump-enriched and the opening displacements are censored and passed into VCCT for G calculation. The black circles show the location of regular jump-enriched nodes inside the crack opening region.

The bottom three plots shows the GI/GII/GIII, respectively, along the crack front, starting with the radius angle, theta = 0. Since this is a shear-dominant case and the crack is partially closed, the GI is zero for certain range of theta. The G values predicted from X-FEM match very well with the double-node model using brute-force VCCT calculation. The difference between two models is well below 1%.

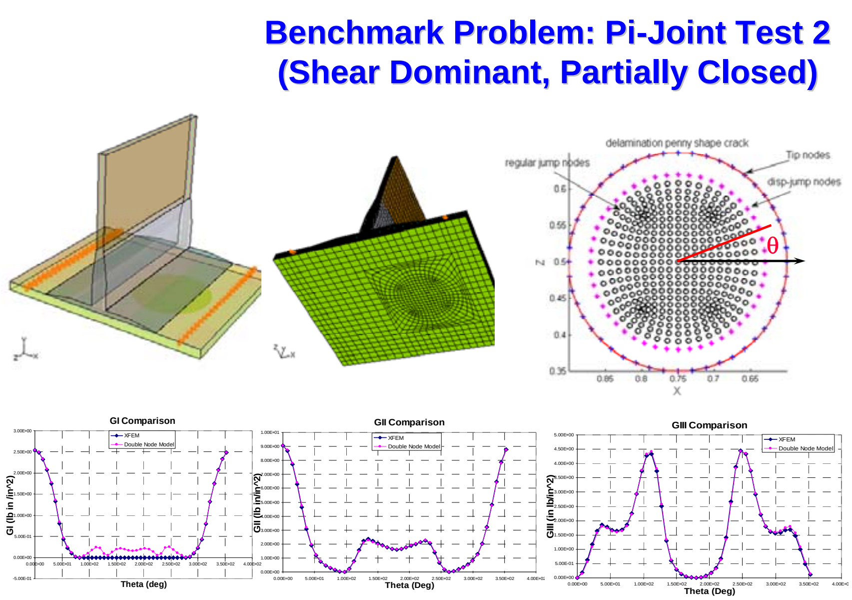

Figure 14: Verification of G Prediction comparing XFEM vs Double-Node Model Using the Same Mesh Design.

From the cut view of crack deformed shape (Figure 15), the crack surfaces are partially penetrated to each other.

The results presented so far do not consider the crack surface over-closure. In fact, the surface penetration can be seen in the crossed-sectional view of the model's deformed shape in Figure 15.

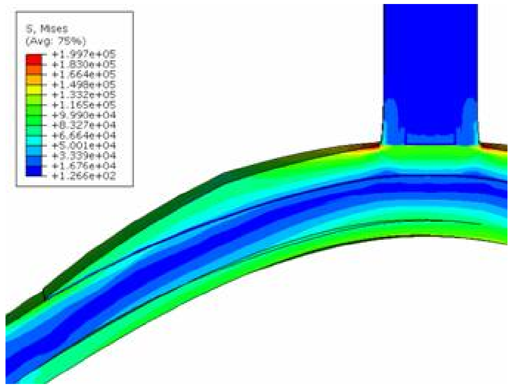

Figure 15: Cut View of Cracked Composite Joint in its Deformed Shape

The comparison between the non-contact results (Gs) vs. the results with contact (Gs-C) are plotted in Figure 16. The shear mode, GII has maximum 20% of difference.

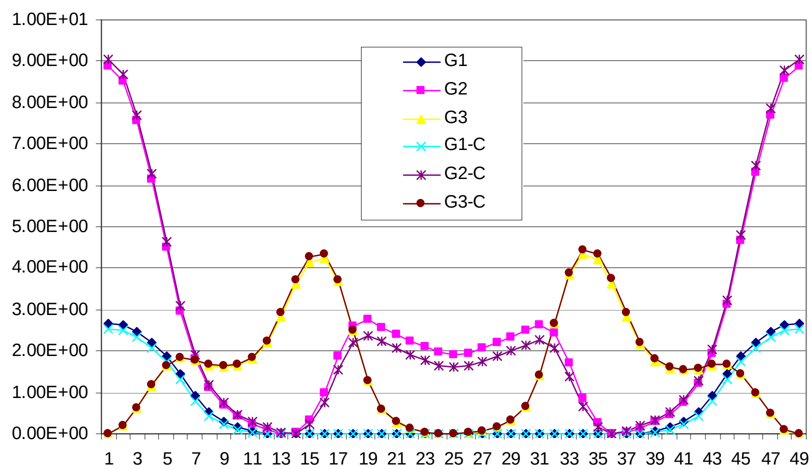

Figure 16: Prediction of G Components along Circular Crack Front and Effect of Crack Surface Contacts

If we choose GIc=6.3 in lb/in2 and GIIc=GIIIc=4.8 in lb/in2, using the power-law criterion of GI/GIc+GII/GIIc+GIII/GIIIc, the total G along the crack front can be viewed in the following Figure 17.

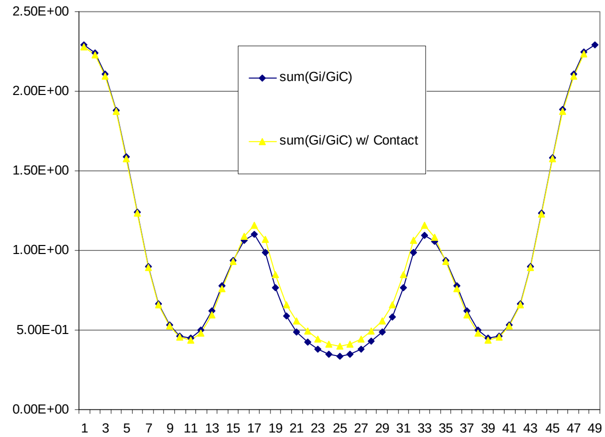

Figure 17: Total G Prediction and Effect of Crack Surface Contact.

This figure shows that there is about 17% of difference in total G if the crack surface contact is considered.

4.3 Validation 3: Effect of embedded delamination damage to a nearby edge crack

This example demonstrates multiple cracks being inserted into the existing composite joint model and verifies the convergence of the G prediction with different density of meshes. The geometry of the Pi-joint model and the two cracks are given in Figure 18.

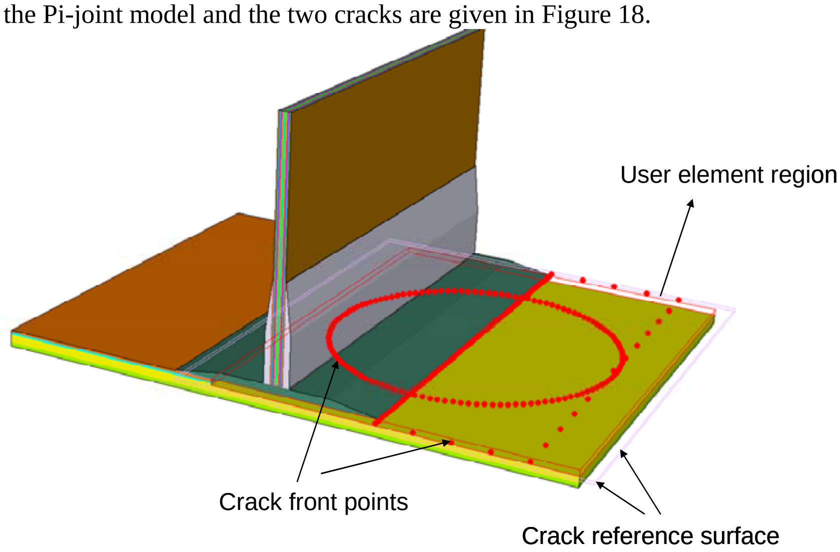

Figure 18: Pi-Joint Abaqus Model with a circular delamination and a rectangular edge crack.

The following figure shows the FMM sub-regions corresponding to the two cracks and the level set values the corresponding regions.

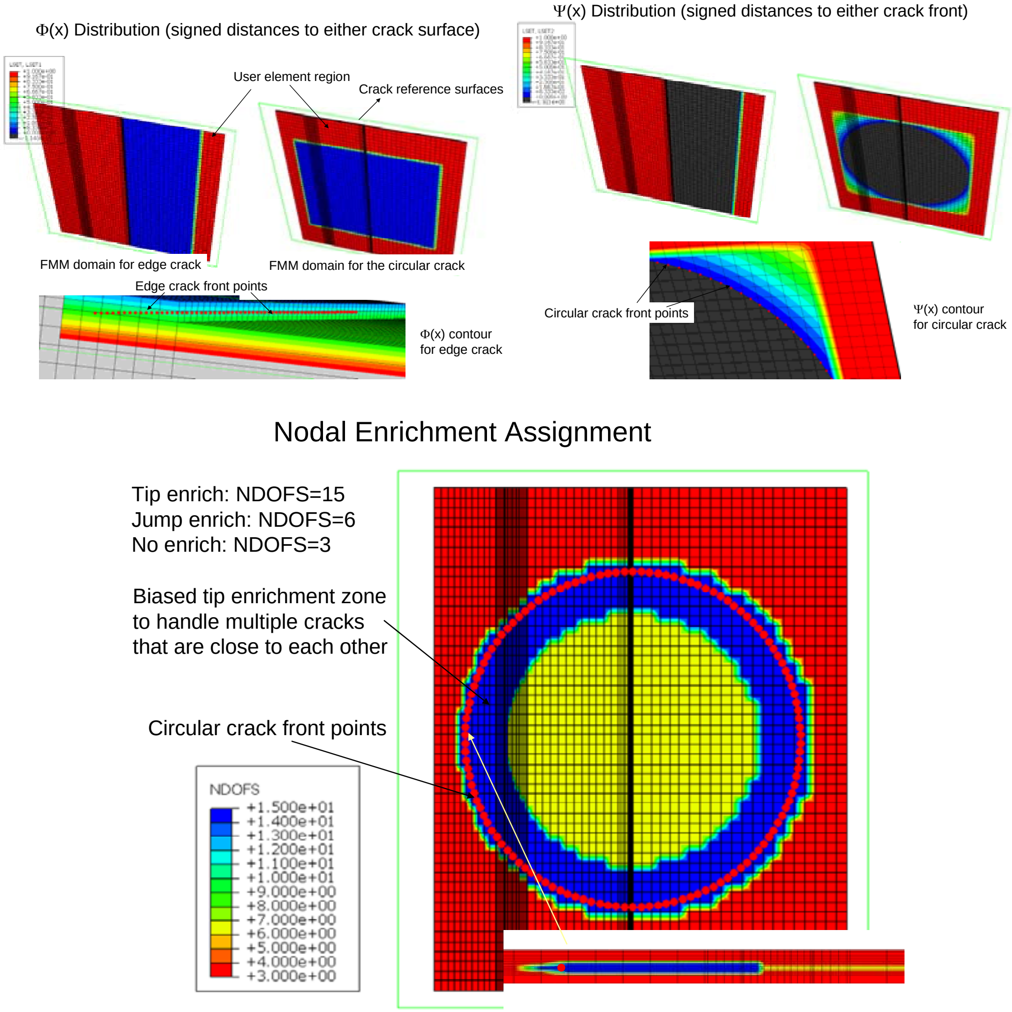

Figure 19: Automatic Zoning of FMM Sub-Regions, Level Set Initialization, and Nodal Enrichment Assignment.

Figure 20 shows the stress components and the crack opening of the damage Pi-joint.

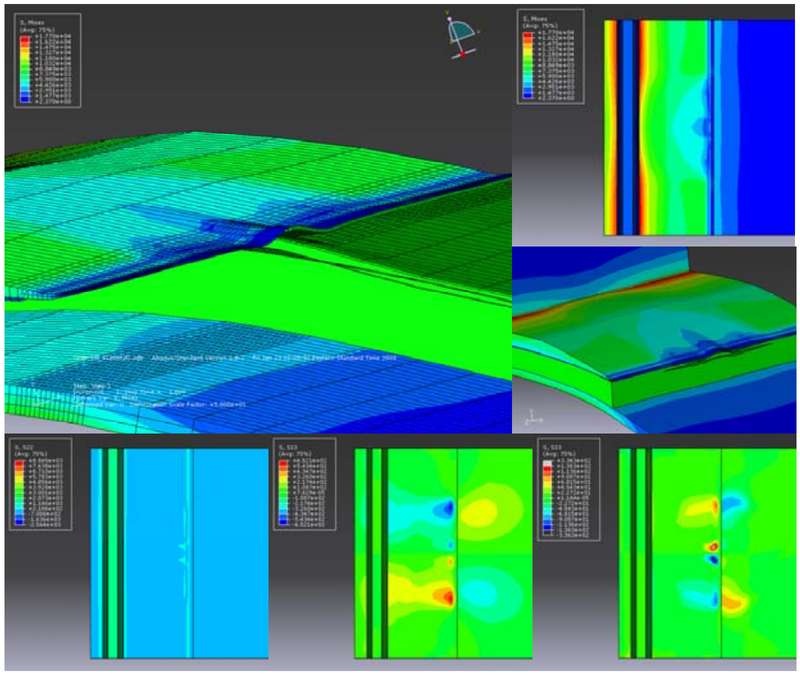

Figure 20: stress components and the crack opening of the damage Pi-joint.

In Figure 21 the predictions of G components are compared with different mesh seeds (15, 20, and 60 seeds) along Pi-joint's width direction. The maximum G is located at the inter-section point of the two cracks. Inside the circular crack region, there seems to be a local buckling in the edge crack flange, this has caused a flat step in the G curves. The flat region corresponds to the maximum shear mode shown in the s13 (in-plane shear) and s23 (out-of-plane shear) in Figure 20.

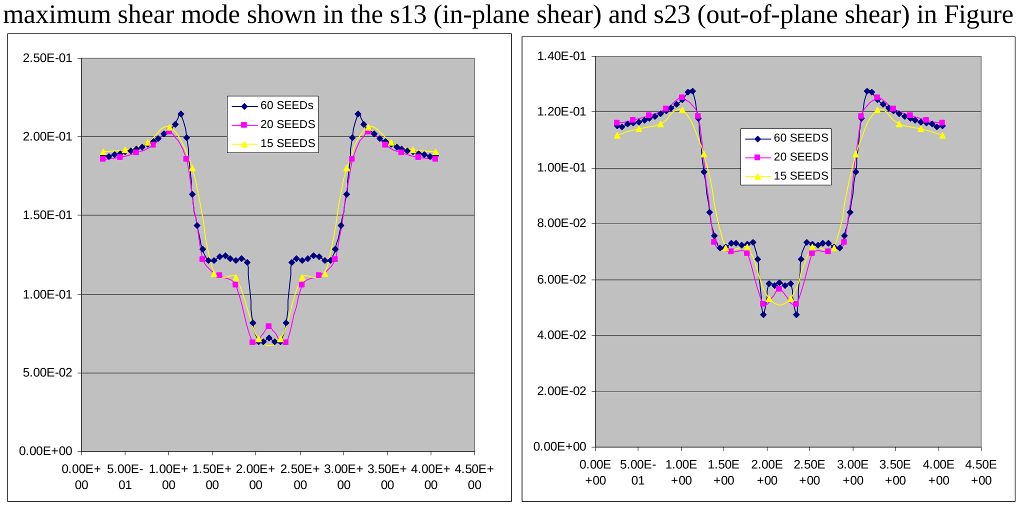

Figure 21: predictions of G components are compared with different mesh seeds

For a complicated fractured model such as this one, we have achieve a converged solution using relatively coarse, structure mesh and successfully demonstrates the multiple crack interactions. More detailed analyses also shows that the effects of the embedded delamination can vary significantly, as the distance between the two crack changes. Indeed, the delamination crack can change from opening to penetration (where contact constraint needs to be enforced), depending on the distance and the material stiffness ratio between the crack interface.

5. Conclusion

Global Engineering & Materials, Inc has developed an add-on X-FEM toolkit for Abaqus (XFA) that works seamlessly with the common commercial, off-the-shelf (COTS) version of Abaqus software suite for an automated crack onset and growth prediction analysis. During the development process, rigorous validation has been made to ensure the tool is robust, accurate and generates high fidelity predictions in the fracture and fatigue analysis The tool has great potential to be used in various designs and analysis practices such as illustrated in the examples. We have scheduled to release this tool in summer 2009. Support from the Air Force SBIR program and our industry partners, including SIMULA of Dassault Systems, LM Aero, and Bell Helicopter are highly acknowledged.

6. References

1. Belytschko T, Black T, "Elastic crack growth in finite elements with minimal remeshing", International Journal for Numerical Methods in Engineering, 45, 601-620, 1999.

2. Jay Shi, Jim Lua, Haim Waisman, Phillip Liu, Ted Belytschko, N. Sukumar, and Yu Liang, "X-FEM Toolkit for Automated Crack Onset and Growth Prediction", AIAA Proceedings, 2008.

3. Miranda, et al., Fatigue life and crack path predictions in generic 2D structural components, Engineering Fracture Mechanics 70 (2003) 1259–1279

4. Moës, N, Dolbow, J, Belytschko, T., "A finite element method for crack growth without remeshing", International Journal for Numerical Methods in Engineering, 46, 131-150, 1999.

5. Sukumar, N, Moës, N, Moran, B, Belytschko T., "Extended finite element method for three-dimensional crack modeling", International Journal for Numerical Methods in Engineering, 48, 1549-1570, 2000.

6. Ventura G., E. Budyn, T. Belytschko, Vector Level Sets for Description of Propagating Cracks in Finite Elements. International Journal for Numerical Methods in Engineering, 58 (2003) pp. 1571–1592.